

光学学报

基于空间编码结构光源的 2 bit 光控可编程太赫兹超表面

戴耀威^{1,2}, 陈聪², 高鹏², 赵佳明², 路祥宇², 万寅辉², 王馨艳², 赵思怡², 刘海^{1,2*}

¹中国矿业大学教育部地下空间智能控制工程研究中心, 江苏 徐州 221116;

²中国矿业大学信息与控制工程学院, 江苏 徐州 221116

摘要 设计了一种可由空间编码结构光控制的多功能太赫兹超表面单元, 该单元由嵌有光敏半导体材料的金属裂环-二氧化硅介质层-金属底板组成。超表面单元通过结构光源的编码控制光改变单元顶层金属裂环内嵌光敏半导体的电导率来模拟不同形状的 C 形环, 实现了具有 2 bit 相位编码的光控超表面单元设计。将超表面单元组成阵列, 通过编码结构光的空间分布进一步实现了角度可控的异常反射, 并获得不同阶数的涡旋波束。所提出的基于空间编码结构光源的新型太赫兹超表面光控方式解决了现有光控超表面功能单一、加工难度大等问题, 为光控可编程太赫兹超表面技术发展提供了新的思路。

关键词 表面光学; 太赫兹; 光控超表面; 可编程超表面; 结构光; 波束控制

中图分类号 TN82 文献标志码 A

DOI: 10.3788/AOS222094

1 引言

太赫兹波前调控作为太赫兹技术应用的重要前提成为该领域的研究热点。自崔铁军院士团队提出数字超材料^[1]概念以来, 超材料调控电磁波波前的能力和自由度得到很大提高。超表面是由微结构排列组合而成的二维超材料, 具有轻薄、柔性、易加工等特点, 在器件集成等方面具有明显的优势^[2]。可编程超表面可以通过光、电激励或利用温度敏感的相变材料对超表面单元的幅相特性进行调控^[3-4]。电控超表面一般采用二极管加载在特殊金属结构的两端并通过外加电源的方式实现单元调制, 但受限于二极管器件的结构特性, 电控方式很难应用在太赫兹频段。 $\text{Ge}_2\text{Sb}_2\text{Te}_5$ (GST)与 VO_2 等相变材料的温控超表面可通过温度使相变材料切换状态, 从而改变超表面对于电磁波的响应^[5-6], 但温控超表面需要精确控制环境温度, 且相变材料切换状态需要一定的时间, 这使得温控超表面对于太赫兹波的调制效率不高^[7]。光控超表面的出现可以很好地解决以上问题。

现有大多数光控超表面采用大范围泵浦光激发光敏材料, 改变光敏材料的物理参数, 从而实现超表面功能的转换。目前光控太赫兹超表面可以实现完美吸收与反射功能切换^[8]、利用钙钛矿材料实现可调谐的太

赫兹超表面^[9]、采用结构光源实现可调太赫兹吸收器^[10]等功能。但是上述超表面不能通过光控实现对单个单元的精确控制, 或者仅能调控超表面单元的幅值特性。超表面单元相位控制的缺失导致这些超表面不能采用数字超材料理论对阵列进行编码, 从而灵活控制太赫兹波前。这也是目前光控超表面相较于电控超表面最主要的劣势。2022 年东南大学团队在超表面背面集成光电池, 从而获得光控可编程超表面^[11]。但是这种光-电转换的控制方式需要集成光电池等电路元件, 但这些元件无法集成在小尺寸的太赫兹超表面上, 因此这种控制方式仅适用于微波超表面。

空间编码结构光作为一种特殊的光源, 已经得到广泛应用^[12-13], 常用于智能手机解锁、辅助驾驶雷达等。编码结构光源可以通过定制的微透镜阵列或使用特殊的超表面结构生成。本文采用空间编码结构光和光敏半导体材料, 将光控和数字编码超材料理论相结合, 解决现有光控超表面功能单一的问题。本文通过改变结构光编码的方式来控制超表面顶层金属裂环中光敏半导体的电导率, 模拟不同形状的 C 形环, 实现了交叉极化波相位的 2 bit 编码; 结合广义斯涅尔反射定律^[14], 使用数字超材料理论对阵列进行设计, 验证了所设计超表面单元可以灵活控制太赫兹波前。值得注意的是, 本文的太赫兹超表面加工工艺和现有硅光互补

收稿日期: 2022-12-05; 修回日期: 2023-01-06; 录用日期: 2023-02-09; 网络首发日期: 2023-02-16

基金项目: 国家自然科学基金(51874301)、国家重点研发计划(2021YFC2902702)

通信作者: *lhai_hust@hotmail.com

金属氧化物半导体(CMOS)工艺完全兼容^[15]。

2 超表面单元结构与响应

反射型超表面主要由不同图案的金属顶层、介质层及底层金属反射板组成^[16]。超表面顶层金属图案的设计是超表面调节反射波幅相特性的关键。常见的太赫兹谐振型超表面顶层图案为纳米金属棒^[17]和开口谐振环^[18-21],以及由这两种结构组成的复杂图形^[22]。其中开口环结构简单,对入射波的幅相特性都有良好的调制效果,常被用于超表面设计。基于金属裂环和光敏半导体材料设计了一种由空间编码结构光控制的等效开口谐振环太赫兹超表面单元。

图1(a)所示的基本结构由空间编码结构光源和

超表面单元组成,图1(b)所示的单元基本结构自顶层开始依次为嵌入光敏锗材料的金属裂环、二氧化硅(SiO_2)介质层以及底层金属反射板。该单元中所有的金属均为铜,其电导率为 $\sigma_{\text{Cu}} = 5.96 \times 10^7 \text{ S/m}$,二氧化硅的介电常数为 $\epsilon_{\text{SiO}_2} = 3.9$,锗的介电常数为 $\epsilon_{\text{Ge}} = 16.6$ 。每块光敏锗材料的正上方对应一个空间编码结构光源,该空间编码结构光源用于控制对应光敏锗材料的电导率,以模拟不同连接状态的金属裂环。二氧化硅被选作超表面介质层材料,不仅是因为其在太赫兹波段具有良好的性能^[23],还因为金属-二氧化硅-金属组成的结构为现有硅光CMOS工艺的常用结构。

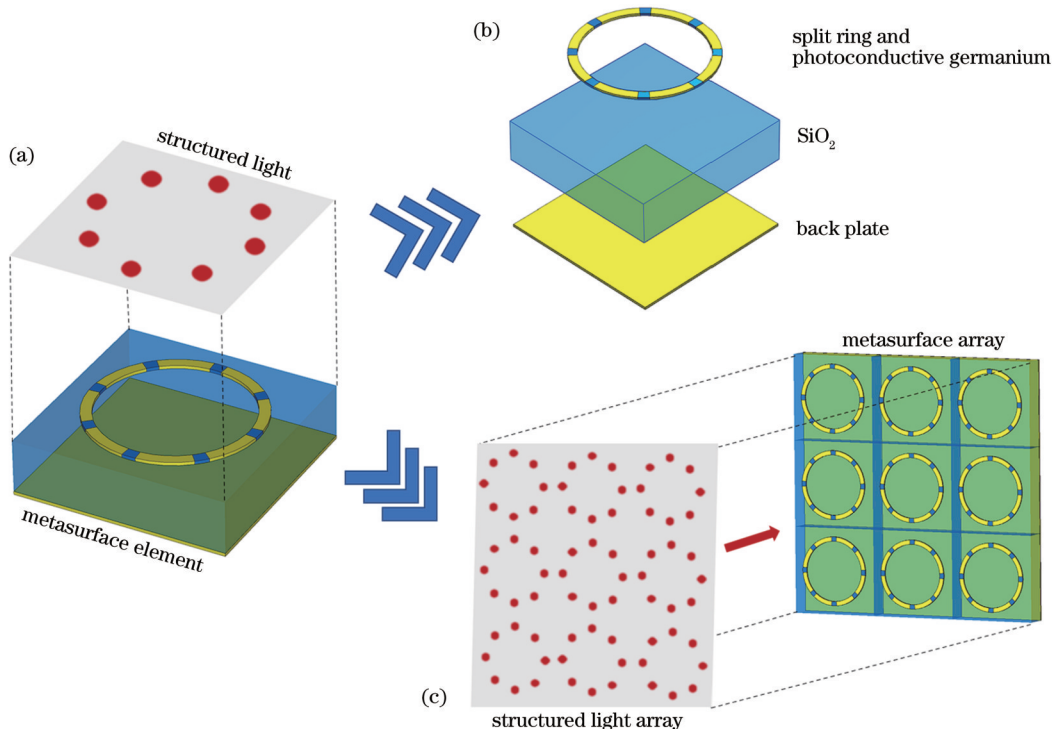


图1 超表面单元与阵列模型。(a)超表面单元和结构光源;(b)超表面单元层结构示意图;(c)空间编码结构光控制示意图

Fig. 1 Metasurface element and array model. (a) Metasurface element and structured light; (b) schematic of metasurface element layer structure; (c) schematic of spatially encoded structured light control

所设计的超表面单元尺寸如图2所示。超表面单元的周期 $l = 40 \mu\text{m}$,顶层和底层金属厚度 $t_m = 0.6 \mu\text{m}$,顶层金属裂环的外径和内径分别为 $R_o = 16 \mu\text{m}$ 、 $R_i = 14 \mu\text{m}$ 。金属裂环内嵌的光敏锗材料以 45° 角均匀排列,其角度 $a = 8^\circ$, SiO_2 介质层厚度 $h = 10 \mu\text{m}$ 。

空间编码结构光和光敏锗材料是超表面单元能实现2 bit相位编码的关键。光敏锗材料可以被1600 nm及以下波长的控制光激发^[24],本实验采用波长为1550 nm的编码结构光源。当光照能量超过光敏半导体的带隙能量时,载流子密度增大,光激发的载流子密度随着泵浦光能量的增加而增大,其寿命大约为几百

纳秒,相较于太赫兹脉冲的持续时间要长很多,而泵浦光与太赫兹光束之间的时间延迟可以保证载流子的相对稳态^[25]。因此,通过改变结构光源的编码状态可以调节光敏锗的电导率,使其在绝缘态和金属态之间转换。

光敏锗的状态可以通过不同的空间编码结构光进行改变,从而对整个裂环的形态进行编程与控制^[26]。如图3(a)所示,对单元结构进行数字化处理,将一个单元内的编码结构点光源和光敏锗材料采用LSB(least significant bit)的形式进行二进制编码,超表面单元光敏锗的编号同样代表该超表面单元对应的上层结构光点光源的编号。规定0为所处位置的光敏锗材

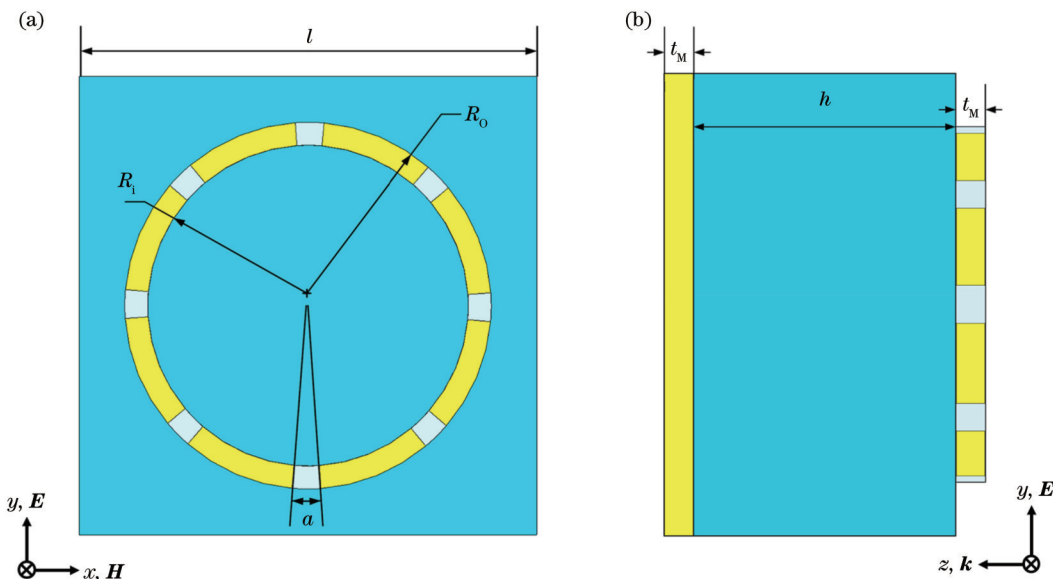


图2 超表面单元尺寸。(a)超表面单元正视图;(b)超表面单元侧视图

Fig. 2 Schematic of metasurface element. (a) Front view of metasurface element; (b) side view of metasurface element

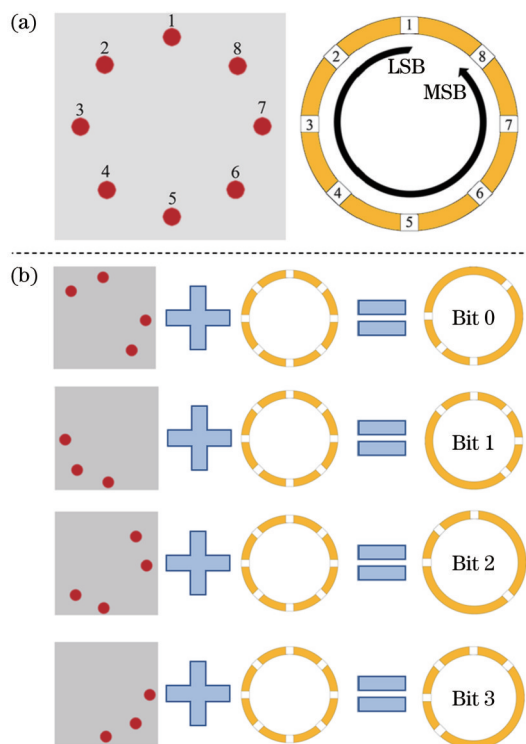


图3 超表面单元编码与等效图。(a)结构光和光敏锗位置编码;(b)金属裂环等效图。

Fig. 3 Coding and equivalence diagrams of metasurface elements. (a) Structured light point source and photosensitive Ge position coding; (b) metal split ring equivalence diagram

料没有被对应的编码结构光激发,对应 $\sigma_{Ge} = 1 \text{ S/m}$;规定1为对应位置的光敏锗材料被激发,对应 $\sigma_{Ge} = 3 \times 10^5 \text{ S/m}$ 。由于不能保证在未激发态时光敏半导体处于完全绝缘的状态,因此不用 $\sigma_{Ge} = 0 \text{ S/m}$ 表示绝缘态光敏锗的电导率。如图3(b)所示,在编码结构光源和光

敏材料的共同作用下,超材料表面金属裂环等效为2 bit相位编码的类C形环,C形环可以通过控制开口方向影响反射波相位,通过开口大小影响反射波幅度^[27]。表1所示为2 bit相位编码的超表面单元光敏锗激发状态,同时也是顶层编码结构光点光源的开关状态。

表1 2 bit 单元对应的光敏锗激发状态

Table 1 Photoconductive Ge excitation state corresponding to 2 bit element

Bit No.	Encoding result
Bit 0	11000110
Bit 1	00111000
Bit 2	00011011
Bit 3	00001110

太赫兹波入射到由结构光和光敏锗编码的裂环结构时,入射波反射场的交叉极化分量的相位和幅度可以根据编码后的金属裂环进行控制^[27]。如图4所示,

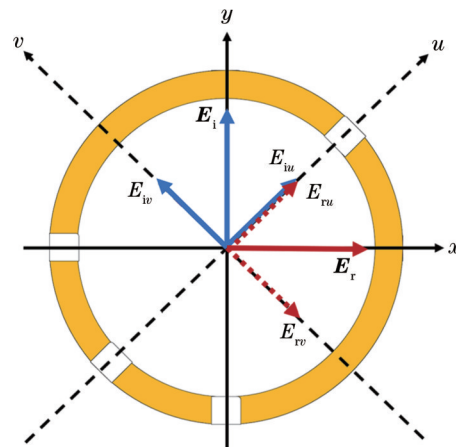


图4 极化转换器工作原理

Fig. 4 Principle of the polarization convertor

以Bit 1编码为例,当 y 极化平面波入射时,其电场矢量可以沿 u 和 v 方向进行分解。 y 偏振入射平面波可以表示为 $E_i = e_u E_{iu} e^{j\phi} + e_v E_{iv} e^{j\phi}$,经过超表面单元反射后反射波同样可以分解为 $E_r = e_u r_u E_{iu} e^{j(\phi + \varphi_u)} + e_v r_v E_{iv} e^{j(\phi + \varphi_v)}$,其中 r_u 和 r_v 分别表示反射场在 u 和 v 方向的反射系数。由于所设计超表面单元沿 u 轴和 v 轴的性质不同,当 u 轴和 v 轴的反射波相差 180° 时,最终合成的电场方向变为 x 方向,实现了入射波经超表面后由 y 偏振至 x 偏振的极化转换。该金属裂环结构还可以尝试更多bit的超表面相位编码组合,下文仅以表1中形成2 bit相位编码的超表面单元为例进行分析。

根据上述分析,使用商业软件CST Microwave

Studio对模型进行仿真,采用频域求解器,边界采用unit cell模拟无限周期单元排列情况下的电磁响应。图5(a)~(d)所示为形成2 bit超表面单元的光敏锗裂环编码示意图,其中黑色方块代表该位置的光敏锗材料被上方的编码控制光激发,白色方块代表该位置的光敏锗材料没有被激发。图5(e)~(h)为形成2 bit相位编码超表面单元对应的空间编码结构光示意图,其中红色点代表波长为1550 nm的点光源。当超表面单元在3.5 THz的频率处实现2 bit相位差时,每个Bit交叉极化参数的幅度几乎相同。其中Bit 0和Bit 2的交叉极化分量均为 -0.91 dB, Bit 1和Bit 3的交叉极化分量均为 -1.19 dB。 y 极化入射波几乎全部转化为 x 极化波,转化效率高。图5(i)~(l)所示为这些金属裂

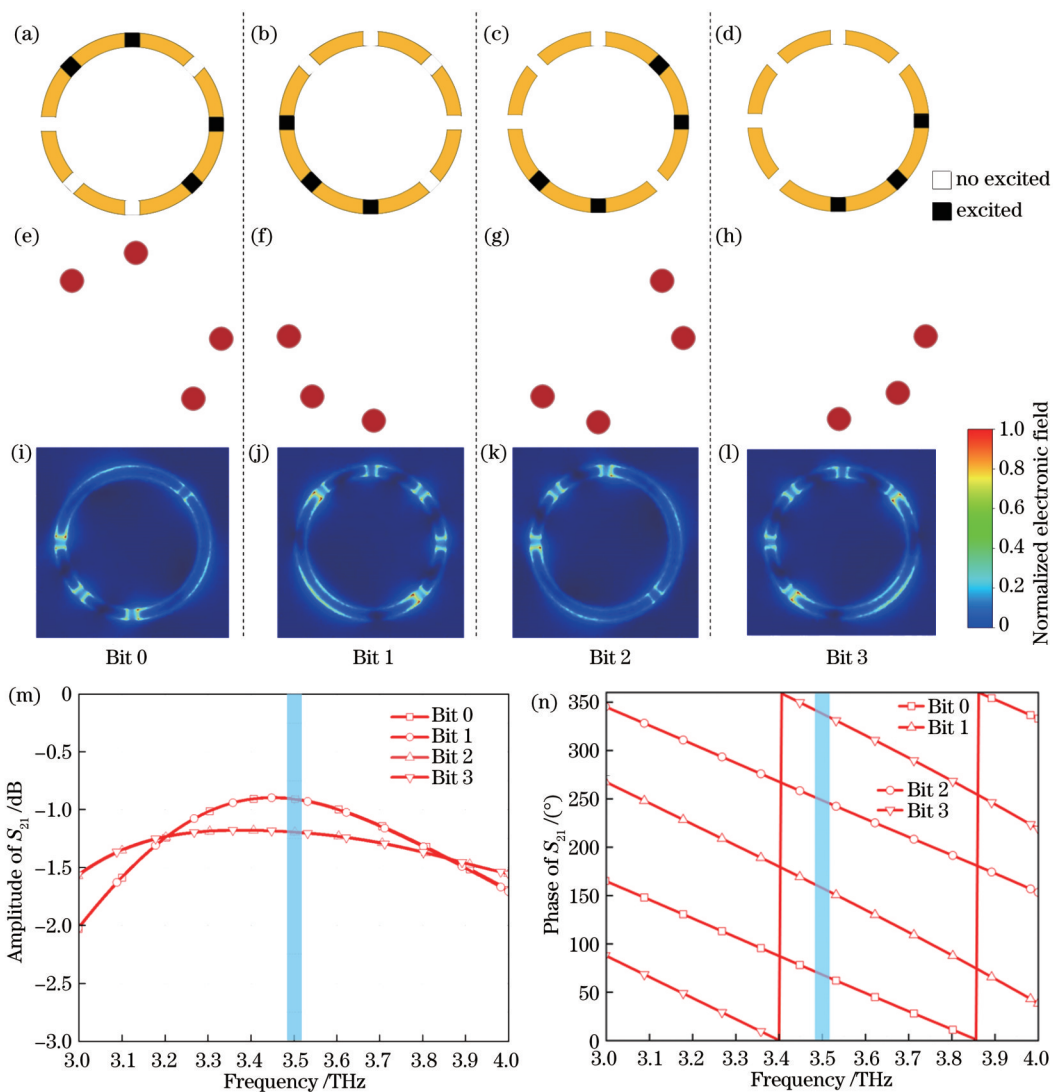


图5 2 bit超表面单元幅相特性。(a)~(d)形成2 bit编码的光敏锗激发状态示意图;(e)~(h)形成2 bit超表面单元结构光编码示意图;(i)~(l)金属裂环和介质交界处的归一化电场;(m)不同结构光编码状态下超表面单元的振幅响应;(n)不同结构光编码状态下超表面单元的相位响应

Fig. 5 Amplitude and phase characteristics of 2 bit metasurface element. (a)–(d) Schematic of the excited state of the photoconductive Ge to form 2 bit code; (e)–(h) schematic of the excited state of structured light to form 2 bit code; (i)–(l) normalized electric field diagram at the intersection of the metal split ring and the dielectric; (m) amplitude and (n) phase response of metasurface element at different excitation states

环在3.5 THz处与介质交界的表面归一化电场,被激发的光敏锗材料由于电导率升高,将原本分开的裂环连接成几组不同大小的金属弧线,在这些弧线的两端电场较为强烈。图5(m)~(n)所示为2 bit所包含的4个单元结构的振幅和相位响应特性,其在3.5 THz处的相位和幅度如表2所示,每个Bit单元之间的相位差约为90°,满足相位编码要求。

表2 2 bit单元在3.5 THz处的相位和振幅

Table 2 Phase and amplitude of the 2 bit element at 3.5 THz

Bit No.	Phase / (°)	Amplitude / dB
Bit 0	68.2	-0.91
Bit 1	157.8	-1.196
Bit 2	248.3	-0.91
Bit 3	337.8	-1.194

3 结果与讨论

为了验证所设计的2 bit相位编码超表面单元,使用2 bit单元结构组成不同的阵列分别实现波束分束、

$$f(\theta, \varphi) = f_e(\theta, \varphi) \sum_{m=1}^N \sum_{n=1}^N \exp \{ -i \{ \varphi(m, n) + kD \sin \theta [(m - 1/2) \cos \varphi + (n - 1/2) \sin \varphi] \} \}, \quad (1)$$

式中: $\varphi(m, n)$ 为每个单元的散射相位; D 为由超表面单元组成的晶格的等效周期; θ 和 φ 分别为超表面散射场的俯仰角和方位角; $f_e(\theta, \varphi)$ 为由超表面单元组成的晶格的模式函数^[1]。根据式(1),可以通过指定的超表面编码方式来控制反射波束的俯仰角(θ)和方位角(φ),其满足

$$\theta = \arcsin \left(n\lambda \sqrt{\frac{1}{\Gamma_x^2} + \frac{1}{\Gamma_y^2}} \right), \quad (2)$$

$$\varphi = \pm \arctan \left(\frac{\Gamma_x}{\Gamma_y} \right), \quad (3)$$

式中: Γ_x, Γ_y 为超表面单元晶格沿 x 和 y 方向排列的周期。如果超表面结构仅存在 x 或 y 方向上的周期性变化,则可将式(2)简化为

$$\theta = \arcsin \left(\frac{nc}{\Gamma f_0} \right) \quad (4)$$

式中: c 为真空中的光速; f_0 为超表面的工作频率; n 为正整数,表示超表面的反射光束可能存在高阶模式,即在主瓣旁会有强度低于主瓣的小型栅瓣。

根据上述理论,使用Bit 0和Bit 2单元对超表面进行以上4种形式的编码^[30-33],分别为0000/0000、2200/2200、222000/222000、22220000/22220000,编码中的数字代表对应的Bit单元,如0代表Bit 0,2代表Bit 2。图6(a)~(d)为这4种编码方式对应的远场,图6(i)~(l)为远场波束对应的超表面阵列编码方式示意图。如图6(a)所示,对于0000/0000这种编码方式,所有超

单波束异常反射、涡旋光等功能。使用CST Microwave Studio软件进行全波仿真,超表面阵列边界设置为open (add space)来模拟真实的激励环境。太赫兹源为 y 偏振沿 $-z$ 方向入射的平面波,远场监视器设置在3.5 THz处,探测远场波束和曲线均为在 y 偏振平面波入射的情况下超表面反射场的交叉极化分量即 S_{21} 参数。

3.1 异常反射

利用前文定义的2 bit超表面单元进行编码。使用4种不同相位的单元组成超表面阵列,不同的空间编码结构光导致超表面阵列的编码方式不同,可以实现不同效果的异常反射。4种Bit单元分别以4种不同颜色的方块表示。在此编码下超表面阵列 x 和 y 方向的相位在呈现梯度变化的同时具有均匀的振幅响应,所以正常入射的平面波会以一个或多个倾角形成异常反射^[28-29]。反射波束的角度符合广义斯涅尔定律^[14]。

在平面波的激励下,超表面的远场散射场表达式^[1]为

表面单元具有相同的相位,导致其远场散射场图案近似于金属平面的远场,远场波束集中在0°,没有发生波束分束。2200/2200、222000/222000、22220000/22220000这3组编码方式的主要区别为超表面单元组成阵列时单元晶格周期不同^[34],分别为四周期晶格、六周期晶格和八周期晶格。四周期晶格对应 $\Gamma = 160 \mu\text{m}$,使用仿真软件得到其反射角为32°,与式(4)的计算结果(32.39°)接近,其主瓣3 dB宽度为6.8°,主瓣强度高于第一栅瓣9.8 dB。六周期晶格阵列整体和四晶格周期阵列类似,晶格周期增大,导致 Γ 增大,反射角变小。在六周期晶格阵列中,反射角的仿真结果为20°,与式(4)的计算结果(20.92°)接近,主瓣3 dB宽度为6.3°,主瓣强度高于第一栅瓣9.2 dB。值得注意的是,当晶格周期增大到八周期时,异常反射波束的远场出现高阶栅瓣,其中光束主瓣角度为15.3°,主瓣3 dB宽度为6.1°,栅瓣角度为51.5°,与式(4)的计算结果相符。

使用所设计的全部2 bit相位单元构成超表面阵列时可以实现单波束异常反射。采用3种不同的编码方法,分别为00112233/00112233、000111222333/000111222333、0000111122223333/0000111122223333。这3种编码方式的远场图案如图7(a)~(c)所示,超表面单元排布方式如图7(g)~(i)所示。使用商业软件CST Microwave Studio对3种编码方式进行仿真,可以得到其单波束异常反射角,分别为15.4°、10.1°、7.4°。图7(d)~(f)所示为使

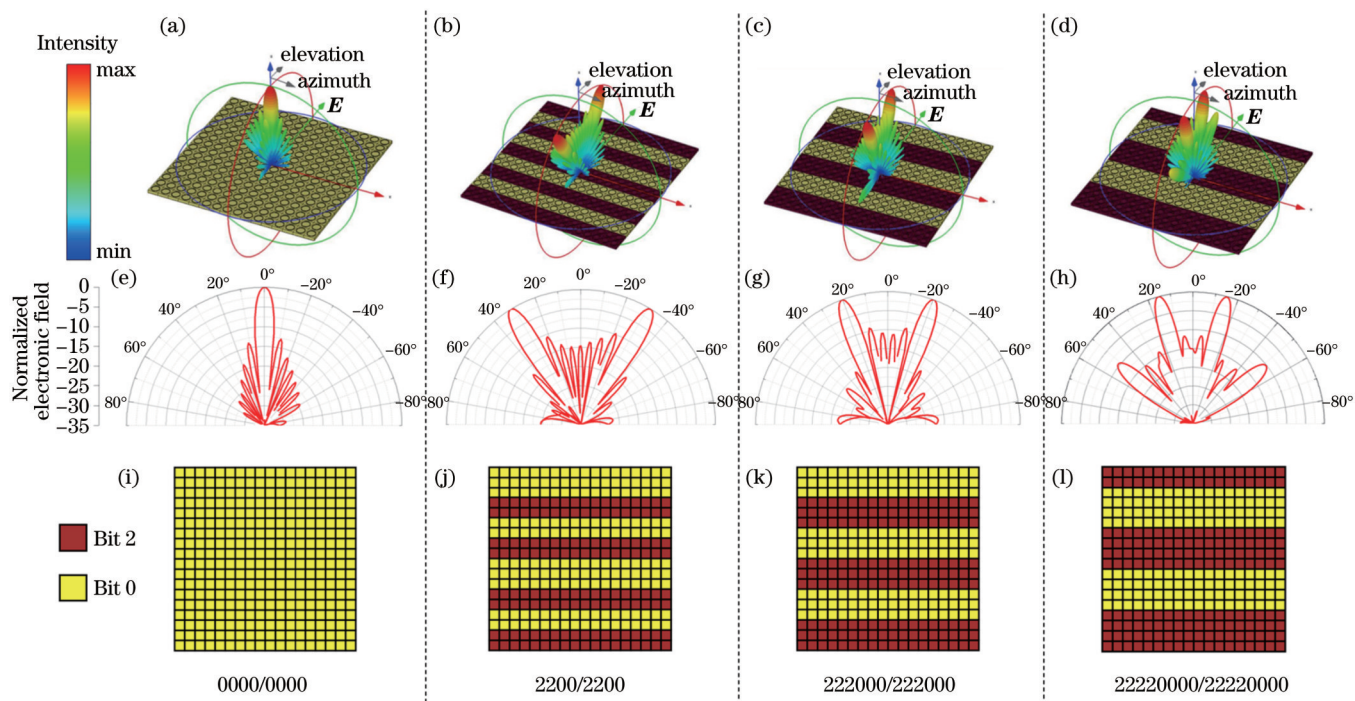


图6 超表面波束分束特性。(a)~(d) 4种编码方式的远场图案;(e)~(h) 4种编码方式的远场波束在 $y=0$ 截面处的电场;(i)~(l) 4种编码方式对应的超表面单元排布方式示意图,所有的超表面阵列均有 18×18 个超表面单元

Fig. 6 Metasurface beam splitting characteristics. (a)–(d) Simulated far-field scattering patterns of the metasurface with four coding sequences; (e)–(h) electric field at $y=0$ cross-section for the far-field beams of four encoding methods; (i)–(l) schematic of the metasurface element layout method, and all metasurface arrays have 18×18 elements

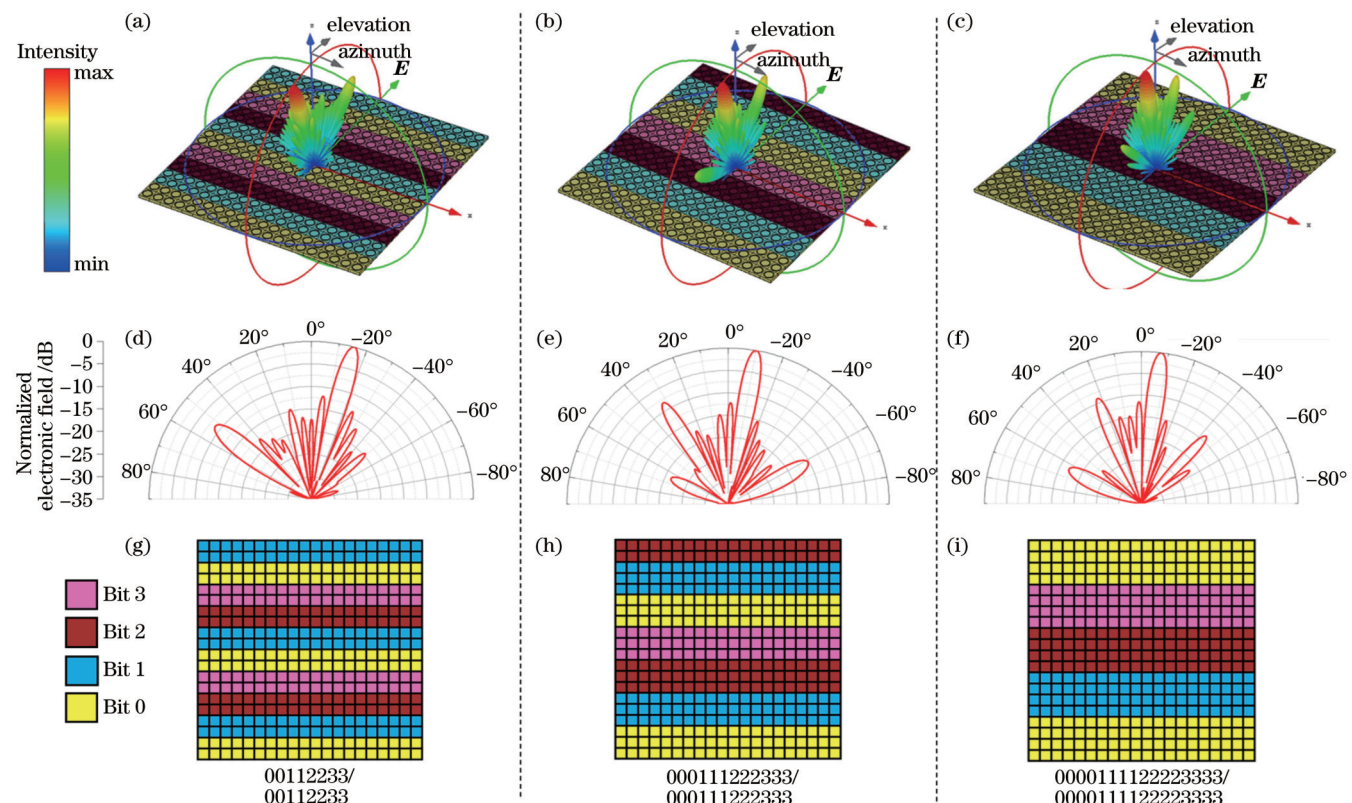


图7 超表面单波束异常反射特性。(a)~(c) 3种编码方式的远场图案;(d)~(f) 3种编码方式的远场波束在 $y=0$ 截面处的电场;(g)~(i) 3种编码方式对应的超表面单元排布方式示意图,所有的超表面阵列均有 20×20 个超表面单元

Fig. 7 Single-beam anomalous reflection characteristics of the metasurface. (a)–(c) Simulated far-field scattering patterns of the metasurface with three coding sequences; (d)–(f) electric field at $y=0$ cross-section for the far-field beams of three encoding methods; (g)–(i) array coding schematic of three encoding methods, and all metasurface arrays have 20×20 elements

用3种编码方式的超表面在 $y=0$ 截面处的远场,可以看到,随着相位梯度编码周期的增大,单波束异常反

射的角度逐渐减小。仿真结果与式(4)的计算结果几乎一致。

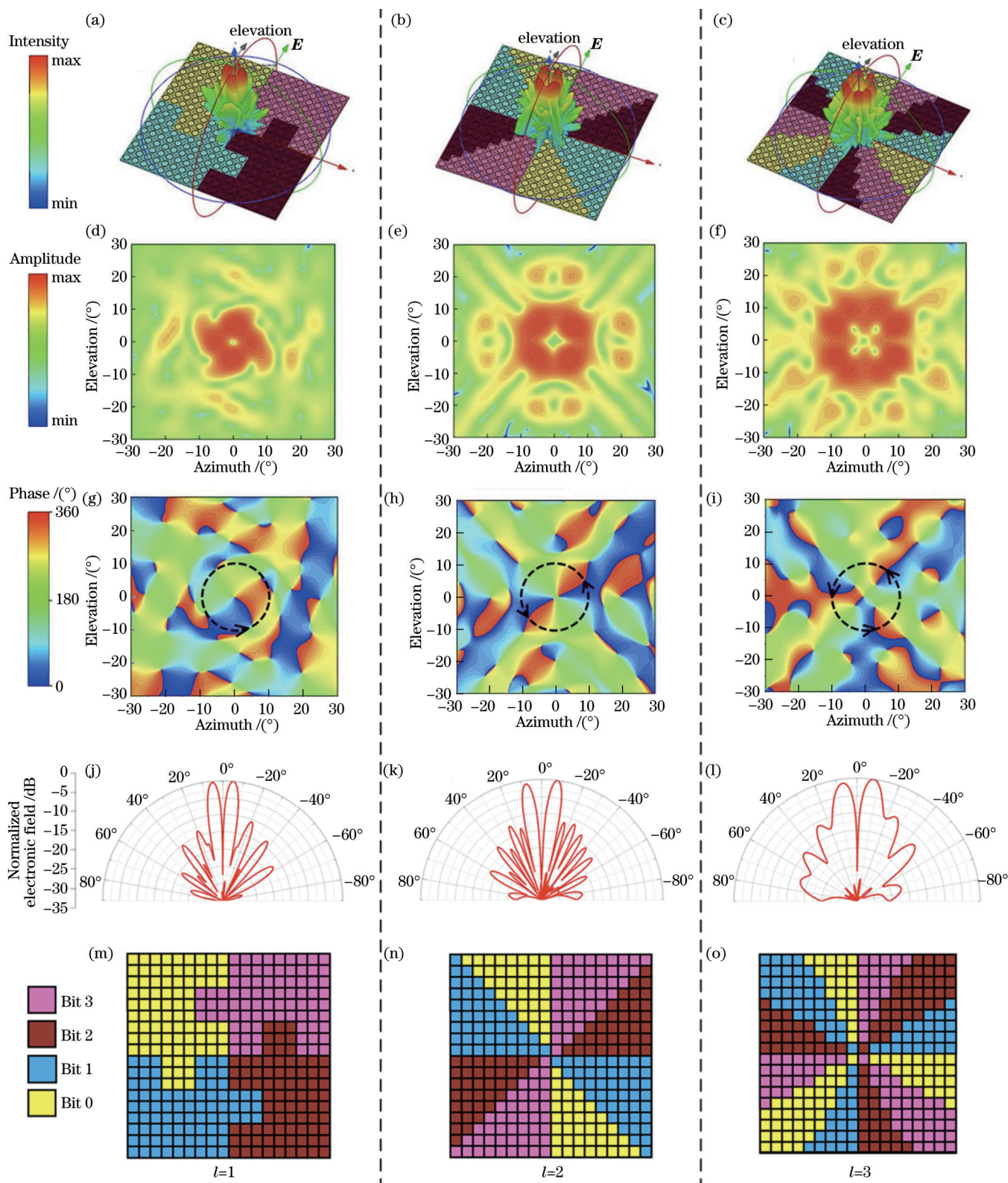


图8 编码超表面生成携带轨道角动量的波束。(a)~(c) $l=1$ 、 $l=2$ 、 $l=3$ 的超表面编码生成涡旋光的远场图;(d)~(f)生成涡波束的幅度;(g)~(i)涡旋波束的相位分布;(j)~(l)涡旋波束在 $x=0$ 截面处的远场;(m)~(o)涡旋光束超表面编码示意图

Fig. 8 Encoded metasurface generation of beams carrying OAM. (a)–(c) Far-field patterns of $l=1$, $l=2$, and $l=3$ metasurface encoding generation of vortex light; (d)–(f) generated vortex beam amplitude; (g)–(i) generated vortex beam phase; (j)–(l) far field at the $x=0$ cross-section of vortex beam; (m)–(o) schematic of three orders of vortex beam metasurface encoding

3.2 涡旋波束

轨道角动量作为电磁波的基本属性,在提升系统通信效率和容量方面有着极大的应用价值。携带轨道角动量的波束又称涡旋波束,其波前相位呈螺旋状分布^[35]。利用超表面产生涡旋波束较为方便,只要保证超表面单元交叉极化分量的振幅几乎相同,且相位呈现螺旋分布,就能获得携带不同阶轨道角动量的太赫兹波束。本小节使用所设计的超表面单元组成超表面阵列来获得一阶、二阶、三阶涡旋光束。

根据麦克斯韦电磁场理论,电磁波角动量J可以分解为自旋角动量S和轨道角动量L。

$$J = S + L, \quad (5)$$

$$S = \epsilon_0 \int \operatorname{Re} \{ E^* \times A \} dv, \quad (6)$$

$$L = \epsilon_0 \int \operatorname{Re} \{ iE^* [-i(r \times \nabla) \cdot A] \} dv, \quad (7)$$

式中: A 表示矢量位函数; E 为电场强度; ϵ_0 为介电常数; r 为光子的位置矢量。从上述公式可以看出自旋角动量S与波束位置无关。采用y极化平面波作为太赫兹源,其自旋角动量 $|S|=0$ 。携带轨道角动量的电磁波相位波前为带有阶数的螺旋相位结构。携带轨道角动量的电磁波束可以表示为

$$E(r, \varphi) = A(r)e^{il\varphi}, \quad (8)$$

式中: $A(r)$ 表示振幅; φ 为方位角; l 表示涡旋光阶数, $l=1$ 表示电磁波波前相位沿着波矢中心旋转一周,相位变化为 2π 。高阶涡旋光同理。当平面波入射到超表面阵列时,若要将其转化为 l 阶涡旋光束,超表面的相位分布^[36]可以表示为

$$\varphi(x, y) = l \arctan(y/x), \quad (9)$$

式中:(x, y)为超表面单元的二维坐标。

如图8所示,将2 bit可编程超表面单元按照Bit 0—Bit 1—Bit 2—Bit 3的顺序以超表面中心为轴旋转,可以得到不同阶数的涡旋光束生成表面,一阶涡旋波束为使用4种Bit单元沿超表面阵列中心均匀旋转一周,其相位变化为 2π ,二阶涡旋波束的相位变化为 4π ,三阶涡旋波束的相位变化为 6π 。超表面单元具体排列方式如图8(m)~(o)所示。可编程超表面阵列采用CST Microwave Studio软件进行仿真,其相位仿真结果如图8(g)~(i)所示,可以明显地看出,随着超表面相位编码周期的增加,生成涡旋波束波前的相位呈现相同的变化规律。如图8(d)~(f)所示,产生的涡旋光束的远场为环形分布,中心凹陷,且中心凹陷处的强度均低于主瓣25 dB以上,性能良好。

4 结论

设计了一种基于空间编码结构光的光控太赫兹超表面单元结构。为了验证这种控制方式的有效性,使用这种单元组成超表面阵列,采用数字超材料的理论对超表面进行编码,实现了波束异常反射,并获得不同

阶涡旋波束,且性能优良。

利用空间编码结构光源和光敏半导体材料,通过编码结构光的形式对每个超表面单元的幅相特性进行调控,解决了光控太赫兹超表面单元精确调控的问题。同时成功地将数字超材料理论应用到光控太赫兹超表面上,实现了2 bit相位编码光控太赫兹超表面。通过光控编码不同类型的超表面阵列解决了现有光控超表面功能单一的问题,丰富了光控太赫兹超表面的应用,为光控太赫兹超材料的发展提供了新的思路。

参 考 文 献

- [1] Cui T J, Qi M Q, Wan X, et al. Coding metamaterials, digital metamaterials and programmable metamaterials[J]. Light: Science & Applications, 2014, 3(10): e218.
- [2] Tsilipakos O, Tasolamprou A C, Pitilakis A, et al. Toward intelligent metasurfaces: the progress from globally tunable metasurfaces to software-defined metasurfaces with an embedded network of controllers[J]. Advanced Optical Materials, 2020, 8(17): 2000783.
- [3] Wan X, Qi M Q, Chen T Y, et al. Field-programmable beam reconfiguring based on digitally-controlled coding metasurface[J]. Scientific Reports, 2016, 6(1): 1-8.
- [4] Wu S R, Lai K L, Wang C M. Passive temperature control based on a phase change metasurface[J]. Scientific Reports, 2018, 8(1): 1-6.
- [5] 李辉,余江,陈哲.基于混合石墨烯-二氧化钒超材料的太赫兹可调宽带吸收器[J].中国激光,2020,47(9): 0903001.
- [6] Li H, Yu J, Chen Z. Broadband tunable terahertz absorber based on hybrid graphene-vanadium dioxide metamaterials[J]. Chinese Journal of Lasers, 2020, 47(9): 0903001.
- [7] 杨森,王佳云,张婷,等.温度电压双可控宽带太赫兹极化转换/吸收超表面[J].光学学报,2022,42(8): 0824001.
- [8] Yang S, Wang J Y, Zhang T, et al. Temperature-voltage bi-controllable broadband terahertz polarization conversion/absorption metasurface[J]. Acta Optica Sinica, 2022, 42(8): 0824001.
- [9] Zhang S J, Chen X Y, Liu K, et al. Nonvolatile reconfigurable terahertz wave modulator[J]. Photonix, 2022, 3(1): 1-14.
- [10] Cheng Y Z, Gong R Z, Zhao J C. A photoexcited switchable perfect metamaterial absorber/reflector with polarization-independent and wide-angle for terahertz waves[J]. Optical Materials, 2016, 62: 28-33.
- [11] Chanana A, Liu X J, Zhang C, et al. Ultrafast frequency-agile terahertz devices using methylammonium lead halide perovskites [J]. Science Advances, 2018, 4(5): eaar7353.
- [12] Gong C, Su W M, Zhang Y, et al. An active metamaterials controlled by structured light illumination[J]. Optik, 2018, 171: 204-209.
- [13] Zhang X G, Jiang W X, Jiang H L, et al. An optically driven digital metasurface for programming electromagnetic functions [J]. Nature Electronics, 2020, 3(3): 165-171.
- [14] 白振旭,陈晖,朱智涵,等.金刚石拉曼振荡器首次实现结构光束输出[J].中国激光,2022,49(21): 2116002.
- [15] Bai Z X, Chen H, Zhu Z H, et al. Diamond Raman oscillator achieves first structured beam output[J]. Chinese Journal of Lasers, 2022, 49(21): 2116002.
- [16] 曾欣怡,伍世虔,陈彬.基于混合编码结构光的相移轮廓测量法[J].激光与光电子学进展,2022,59(13): 1312002.
- [17] Zeng X Y, Wu S Q, Chen B. Hybrid-coded phase-shifting profilometry for structured light measurement[J]. Laser & Optoelectronics Progress, 2022, 59(13): 1312002.
- [18] Yu N F, Genevet P, Kats M A, et al. Light propagation with phase discontinuities: generalized laws of reflection and refraction

- [J]. Science, 2011, 334(6054): 333-337.
- [15] Sun J, Timurdogan E, Yaacobi A, et al. Large-scale silicon photonic circuits for optical phased arrays[J]. IEEE Journal of Selected Topics in Quantum Electronics, 2014, 20(4): 264-278.
- [16] Hu J, Bandyopadhyay S, Liu Y H, et al. A review on metasurface: from principle to smart metadevices[J]. Frontiers in Physics, 2021, 8: 586087.
- [17] Grady N K, Heyes J E, Chowdhury D R, et al. Terahertz metamaterials for linear polarization conversion and anomalous refraction[J]. Science, 2013, 340(6138): 1304-1307.
- [18] Ding J, An S S, Zheng B W, et al. Multiwavelength metasurfaces based on single-layer dual-wavelength meta-atoms: toward complete phase and amplitude modulations at two wavelengths[J]. Advanced Optical Materials, 2017, 5(10): 1700079.
- [19] Yan L B, Zhu W M, Wu P C, et al. Adaptable metasurface for dynamic anomalous reflection[J]. Applied Physics Letters, 2017, 110(20): 201904.
- [20] Xu H X, Hu G W, Li Y, et al. Interference-assisted kaleidoscopic meta-plexer for arbitrary spin-wavefront manipulation[J]. Light: Science & Applications, 2019, 8(1): 1-10.
- [21] 张星源, 谷建强, 师文桥. 基于金属裂环谐振器的太赫兹连续域束缚态超表面[J]. 中国激光, 2023, 50(2): 0214001.
Zhang X Y, Gu J Q, Shi W Q. Terahertz metasurface with bound states in continuum based on metal split ring resonator[J]. Chinese Journal of Lasers, 2023, 50(2): 0214001.
- [22] Qi Y P, Zhang B H, Ding J H, et al. Efficient manipulation of terahertz waves by multi-bit coding metasurfaces and applications of such metasurfaces[J]. Chinese Physics B, 2021, 30(2): 024211.
- [23] Gao Y S, Fan Y B, Wang Y J, et al. Nonlinear holographic all-dielectric metasurfaces[J]. Nano Letters, 2018, 18(12): 8054-8061.
- [24] Ji H Y, Zhang B, Wang G C, et al. Photo-excited multi-frequency terahertz switch based on a composite metamaterial structure[J]. Optics Communications, 2018, 412: 37-40.
- [25] Xu Z C, Gao R M, Ding C F, et al. Photoexcited switchable metamaterial absorber at terahertz frequencies[J]. Optics Communications, 2015, 344: 125-128.
- [26] Venkatesh S, Lu X Y, Saeidi H, et al. A high-speed programmable and scalable terahertz holographic metasurface based on tiled CMOS chips[J]. Nature Electronics, 2020, 3(12): 785-793.
- [27] Zhang X Q, Tian Z, Yue W S, et al. Broadband terahertz wave deflection based on C-shape complex metamaterials with phase discontinuities[J]. Advanced Materials, 2013, 25(33): 4567-4572.
- [28] Bao L, Wu R Y, Fu X J, et al. Multi-beam forming and controls by metasurface with phase and amplitude modulations [J]. IEEE Transactions on Antennas and Propagation, 2019, 67 (10): 6680-6685.
- [29] Wan X, Xiao Q, Zhang Y Z, et al. Reconfigurable sum and difference beams based on a binary programmable metasurface [J]. IEEE Antennas and Wireless Propagation Letters, 2021, 20 (3): 381-385.
- [30] Zhang F H, Saifullah Y, Yang G M, et al. 1-bit, 2-bit polarization insensitive reflection programable metasurface[C]// 2018 IEEE International Symposium on Antennas and Propagation & USNC/URSI National Radio Science Meeting, July 8-13, 2018, Boston, MA, USA. New York: IEEE Press, 2019: 1899-1900.
- [31] Zhang X H, Zhang H, Su J X, et al. 2-Bit programmable digital metasurface for controlling electromagnetic wave[C]// 2017 Sixth Asia-Pacific Conference on Antennas and Propagation (APCAP), October 16-19, 2017, Xi'an, China. New York: IEEE Press, 2018.
- [32] Kong X K, Wang Q, Jiang S L, et al. A metasurface composed of 3-bit coding linear polarization conversion elements and its application to RCS reduction of patch antenna[J]. Scientific Reports, 2020, 10(1): 1-10.
- [33] Zhang L, Cui T J. Angle-insensitive 2-bit programmable coding metasurface with wide incident angles[C]// 2019 IEEE Asia-Pacific Microwave Conference (APMC), December 10-13, 2019, Singapore. New York: IEEE Press, 2020: 932-934.
- [34] Fu X J, Shi L, Yang J, et al. Flexible terahertz beam manipulations based on liquid-crystal-integrated programmable metasurfaces[J]. ACS Applied Materials & Interfaces, 2022, 14 (19): 22287-22294.
- [35] Allen L, Beijersbergen M W, Spreeuw R J, et al. Orbital angular momentum of light and the transformation of Laguerre-Gaussian laser modes[J]. Physical Review A, 1992, 45(11): 8185-8189.
- [36] Gao X, Tang L G, Wu X B, et al. Broadband and high-efficiency ultrathin Pancharatnam-Berry metasurfaces for generating X-band orbital angular momentum beam[J]. Journal of Physics D, 2021, 54(7): 075104.

2 bit Optically Controlled Programmable Terahertz Metasurface Based on Spatially Encoded Structured Light

Dai Yaowei^{1,2}, Chen Cong², Gao Peng², Zhao Jiaming², Lu Xiangyu², Wan Yinhu²,
Wang Xinyan², Zhao Siyi², Liu Hai^{1,2*}

¹Engineering Research Center of Intelligent Control for Underground Space, Ministry of Education, China
University of Mining and Technology, Xuzhou 221116, Jiangsu, China;

²School of Information and Control Engineering, China University of Mining and Technology, Xuzhou 221116,
Jiangsu, China

Abstract

Objective Terahertz wavefront manipulation, particularly flexible switching of terahertz wavefronts through programmable metasurface, has good prospects for application. Electricity, temperature, and light control are the most

common programmable metasurface control methods available today. In order to directly modulate an electronically controlled metasurface, diodes loaded on both ends of a particular metal structure are typically powered through an external power supply. However, due to the structural characteristics of the diodes, it is difficult to reduce the cell area for terahertz wave modulation. Temperature-controlled metasurfaces use phase-change materials to change the metasurface's reaction to electromagnetic waves. However, precise control of the ambient temperature is required. In addition, the phase-change material takes time to alter states, which induces the terahertz wave's low modulation efficiency. Optically controlled metasurfaces can integrate photosensitive semiconductors into elements to control the amplitude and phase characteristics of metasurface units by changing the properties of photosensitive materials. However, existing metasurfaces lack accurate optical control of the individual elements, which makes it impossible to modify the wavefront of incident terahertz waves by encoding the elements according to digital metamaterials theory. In this paper, a 2 bit phase-encoded metasurface unit is realized by controlling the conductivity of the embedded photosensitive semiconductor in the top metal split ring of the cell through the encoding of the structural light source to simulate different C-shaped rings. Subsequently, by encoding the spatial distribution of structured light, the developed metasurface units are built into arrays to generate angularly adjustable anomalous reflections and vortex beams of different orders. A new optical control method is proposed here. It is combined with spatially encoded structured light and can efficiently solve the problems of the existing optical control metasurface's single function and high processing difficulty.

Methods In this paper, a metal split ring construction with an embedded photosensitive germanium material is used to imitate the reaction of a C-shaped ring to terahertz radiation. By changing the electrical conductivity of the embedded photosensitive germanium material with the different encoding of structural light, it switches between the metallic and insulated states, thus changing the connection state of the metal split ring on the top layer of the metasurface. The metal split ring with different connection states can polarize the incident terahertz waves while adjusting their phases. In this paper, we realize a metasurface unit with 2 bit phase encoding by finding a suitable encoded structured light. In the next step, we combine the designed 2 bit phase encoded units with digital encoding metamaterial theory to form different metasurface arrays to achieve anomalous reflections at different angles and vortex beams of different orders, thus verifying the correctness of the metasurface cell design.

Results and Discussions The period of the optically controlled metasurface unit designed in this paper is $40\text{ }\mu\text{m}$ (Fig. 2). The 2 bit phase difference at 3.5 THz is achieved by changing the connection state of the metal split ring at the top of the metasurface with the different encoding of structured light. In this study, we digitally encode structured light and photosensitive materials in the form of least significant bit (LSB) (Fig. 3). Bit 0, Bit 1, Bit 2, and Bit 3 correspond to the codes 11000110, 00111000, 00011011, and 00001110 (Table. 1), respectively. The phases of Bit 0, Bit 1, Bit 2, and Bit 3 at 3.5 THz on the metasurface are 68.2° , 157.8° , 248.3° , and 337.8° , respectively. The amplitude of the cross-polarization of metasurface units is approximately the same while forming a 2 bit phase difference. The amplitudes of Bit 0, Bit 1, Bit 2, and Bit 3 at 3.5 THz are -0.91 dB , -1.196 dB , -0.91 dB , and -1.194 dB , respectively (Table. 2). In this paper, Bit 0 and Bit 2 are selected to form arrays with different lattice periods to achieve a double-beam splitting with beam splitting angles of 32° , 20° , and 15.3° (Fig. 6). Next, a single-beam anomalous reflection is achieved by selecting all bit units to form 8, 12, and 16 lattice metasurface arrays with reflection angles of 15.4° , 10.1° , and 7.4° (Fig. 7), respectively, and the angle decreases with increasing phase gradient encoding period. The vortex beam has a wide range of applications, including increasing system communication efficiency and capacity convenience. The 1st-order, 2nd-order, and 3rd-order vortex beams are realized by different spiral phase encoding methods (Fig. 8), and the beam center depressions are all more than 25 dB below the main flap, with good performance.

Conclusions In this paper, a novel optically controlled metasurface method based on encoded structured light is presented. The combination of spatially encoded structured light and photosensitive semiconductors achieves independent amplitude phase tuning of the optically controlled metasurface unit. The problem of precise tuning of the optically controlled terahertz metasurface unit is solved. In this paper, the 2 bit phase encoded optically controlled terahertz metasurface is realized by combining the digital metamaterial theory. With the theory of digital metamaterials, anomalous reflections at different angles and vortex beams of different orders are achieved by different encoding methods, which realizes the flexible modulation of terahertz wavefront and enriches the application of optically controlled terahertz metasurfaces, and a new idea for developing optically controlled metasurfaces is provided.

Key words optics at surface; terahertz; optically controlled metasurface; programmable metasurface; structured light; beam steering